Spark Plasma Sintering and Optical Characterization of Lunar Regolith Simulant

Roberta Licheri[1], Roberto Orrù[1], Elisa Sani[2*], Aldo Dell'Oro[3], Giacomo Cao[1]

[1]*Dipartimento di Ingegneria Meccanica, Chimica e dei Materiali, Unità di Ricerca del Consorzio Interuniversitario Nazionale per la Scienza e Tecnologia dei Materiali (INSTM) - Università degli Studi di Cagliari, via Marengo 2, 09123 Cagliari, Italy*

[2]*CNR-INO Istituto Nazionale di Ottica, Largo E. Fermi, 6, I-50125 Firenze, Italy*

[3]*Istituto Nazionale di Astrofisica (INAF), Osservatorio Astrofisico di Arcetri, Largo E. Fermi, 5, I-50125 Firenze, Italy*

**Corresponding author, email: elisa.sani@ino.cnr.it*

https://doi.org/10.1016/j.actaastro.2022.09.016

Abstract
To satisfy the essential needs, including energy requirements, for human and robotic space explorations on planetary objects like Moon, Mars and asteroids, the proper exploitation of resources available *in-situ* represents a crucial issue. Along this line, the present work investigates the potential of a sintered lunar regolith simulant (JSC-1A) for possible solar energy harvesting and thermal energy storage applications. Regolith simulant powders are first consolidated by Spark Plasma Sintering (SPS) at 700 and 900°C to produce bulk samples with different relative densities, i.e. 86 and 98%, respectively, and surface porosities. Only modest changes from the compositional point of view are induced by SPS according to XRD analysis. The optical properties of sintered samples and pristine regolith powders are compared, considering the spectral absorptance/emittance, the integrated solar absorptance and the integrated thermal emittance estimated in a temperature range representative for the ISRU application, i.e. from 100 to 1300K. We found that sintering changes the optical properties of regolith in a process-dependent way, with an increased solar absorptance and thermal emittance shown by sintered pellets with respect to pristine powders.

Keywords: ISRU; Lunar regolith; Regolith simulant; SPS; Optical properties; Solar absorber.

1. Introduction

Regolith-covered surfaces exist in several planetological environments. Regolith is a natural by-product where collisional processes dominated by micro-meteorite bombardment and other space weathering mechanism are at work. The surfaces of the Moon and asteroids, being characterized by the absence of any kind of atmosphere, are constantly impacted by a flux of meteoroids and micro-meteoroids able to produce a progressive grinding of surface material.

As for the Moon, the lunar surface, due to the high solar irradiance on it, shows advantageous conditions for solar energy harvesting, once a proper site choice is carried out [1]. However, due to the length of lunar days/nights, energy storage as well is a major issue to be faced. Thermal energy storage (TES) appears the most suitable energy storage approach for future extra-terrestrial human colonies or robotic stations. Regolith, and in particular regolith processed into solid bulks to enhance its thermal properties, is then considered the most natural TES candidate materials [2], [3].

As for asteroids, they have been identified as possible targets for In-Situ Resources Utilization (ISRU), for instance, but not exclusively, for mining purposes [4]–[6]. Studies based on spectroscopic remote analysis and radar observations lead to the conclusion that single metal-rich near-Earth asteroids (NEAs) contain large amount of Fe, Ni, Co, and platinum group metals exceeding the total reserves present on our planet [7], [8]. However, the physical properties of asteroids surface material are not clearly determined yet. Hints about physical properties of asteroid surfaces are generally inferred indirectly from ground-based observations, and only in few cases are obtained from in-situ space missions. Physical parameters of regolith covering asteroid surface seems to depend on the location and dimension of the objects. The cosmic environments of Near-Earth Asteroids and Moon are similar in terms of meteoroid bombardments and solar wind exposure. Their typical meteoroid impact velocities are of the order of 15 km/s, entailing melting and vaporization processes during regolith formation. Instead, mean impact velocities among Main Belt Asteroids, twice to four times as far from the Sun as the Earth, are of the order of 5 km/s [9], [10], involving a different mechanism for regolith formation, i.e. mechanical brecciation. Besides boundary conditions determined by the cosmic environment, properties of the regolith existing on asteroids depend strongly on their dimensions. From one hand, negligible gravity with respect to Moon surface allow a larger regolith mobility and mixing. Moreover, depending on the target and impactor masses, impacts can generate seismic process, thus modifying the distribution of the surface material. On the other hand, regolith maturity degree, as well as surface thermal inertia, could be related to asteroid sizes. In fact, asteroids with diameter larger than 100 km are characterized by values of thermal inertia of the order of lunar soil, while sub-kilometer asteroid can have thermal inertia one order of magnitude larger, two order of magnitude difference in terms of conductivity [11]. Presumably, such trend is because larger asteroids have developed substantial regolith layers unlike the smaller ones. Besides intrinsic properties of the materials that can be found on asteroid surfaces, it is important to underline that the conditions of their exploitation for ISRU applications are substantially different with respect to the lunar environment. For instance, typical rotational period of asteroids are few hours, requiring a significantly different

approach in solar energy harvesting and energy storage. However, being aware of existing differences and once identified the most appropriate simulant, the approach described in this work could be profitably used to evaluate the potential of sintered regoliths in multiple planetological environments.

It is apparent that the development of advanced technologies in the framework of the ISRU concept would certainly provide a strong boost for future human space explorations on Moon, Mars, Near Earth Asteroids, etc. [12], [13]. In particular, the use of regolith resources available in-situ will produce a significant decrease of transportation expenses and a consequent intensification of the manufacturing processes to fabricate constructions and protections resistant to cosmic rays, solar wind and meteoroids, as well other useful installations and apparatuses possibly required, like for instance solar energy harvesting systems and thermal energy storage media. To this aim, efficient technologies to convert natural regolith into bulk bodies are needed. In this regard, various methods, such as pressureless sintering [14], [15], microwave sintering [16]–[18], combustion synthesis based processes [19]–[22], impact procedure [23], high-pressure consolidation [24], spark plasma sintering [14], [25], [26], solar sintering [27]**,** 3D-printing [28]**,** etc., are considered in the literature. To facilitate powder densification, suitable polymers are also used as binders in some investigations [23], [24].

Among the proposed technologies, Spark Plasma Sintering (SPS), also referred to as Electric Current-Assisted Sintering (ECAS), is a widely used efficient consolidation method able to guarantee the obtainment of high densification levels very shortly, compared to standard hot-pressing or pressureless sintering, also when processing highly refractory powders [29].

Because of the limited availability of real lunar soil on Earth, several regolith simulants with similar compositional-structural characteristics have been developed and used in most of the experimental studies above. The only exception is represented by the investigation described in Ref. [17], where Apollo 17 soil was utilized. These simulants include JSC-1A (USA) [19]–[25], [28], JSC-2A (USA) [15], [27], [28], KLS-1 (Korea) [26], and FJS-1 (Japan) [14], [26].

In the present work, taking as case-study a lunar regolith simulant, we are aimed to set a characterization and material property assessment procedure to evaluate the potential of sintered regolith(s) for solar energy harvesting and thermal energy storage in an ISRU perspective.

Indeed, sieved JSC-1A regolith simulant was first characterized from the compositional and thermal stability points of view. Powders are then spark plasma sintered at different temperatures to produce bulk samples with diverse relative densities and surface porosities. The composition, microstructure and optical properties of the resulting materials are investigated. Absorptance of extra-terrestrial solar radiation and temperature-dependent thermal emittance from 100 to 1300K are calculated from experimental spectra, with the aim to evaluate the potential of sintered regolith for energy production and energy storage for ISRU.

2. Materials and method

As provided by the corresponding vendor, the Johnson Space Center Lunar regolith simulant (JSC-1A, Orbital Technologies Corporation, Madison, WI, USA) used in this work consists of a gray material, with a theoretical density of 2.9 g/cm^3 and

melting point in the range 1100º - 1125º C. The related chemical composition is reported in **Table 1**.

***Table 1**. Chemical composition (oxide wt%) of JSC-1A Lunar regolith simulant. It should be noted that the reported composition does not represent actual phases or minerals present in the simulant. The normal convention for data presentation uses oxide formulae from an assumed oxidation state for each element (except for Fe) and oxygen is calculated by stoichiometry.*

Major element composition	**wt. %**
Silicon Dioxide (SiO_2)	46 - 49
Titanium Dioxide (TiO_2)	1 - 2
Aluminum Oxide (Al_2O_3)	14.5 - 15.5
Ferric Oxide (Fe_2O_3)	3 - 4
Iron Oxide (FeO)	7 - 7.5
Magnesium Oxide (MgO)	8.5 - 9.5
Calcium Oxide (CaO)	10 - 11
Sodium Oxide (Na_2O)	2.5 - 3
Potassium Oxide (K_2O)	0.75 - 0.85
Manganese Oxide (MnO)	0.15 - 0.20
Chromium III Oxide (Cr_2O_3)	0.02 - 0.06
Diphosphorus Pentoxide (P_2O_5)	0.6 - 0.7
Sulfur Trioxide (SO_3)	-
Loss on ignition LOI	-

The as received regolith was preliminarily sieved and the resulting –45μm fraction was utilized for additional characterization as well as for producing bulk samples by SPS.

Particle size distribution of the sieved powders was evaluated by a laser light scattering analyser (CILAS 1180, France).

Phases identification in JSC-1A regolith prior and after SPS was carried out by X-ray diffraction (XRD) analysis (RIGAKU Miniflex II diffractometer equipped with a CuKα Ni-filtered radiation).

Thermal stability of lunar simulant from room temperature to 900 °C was evaluated by thermo-gravimetric analysis (TGA) using a simultaneous DTA-TGA Instrument (NETZSCH STA 409PC Luxx, Germany).

The consolidation of regolith powders to obtain bulk samples (about 15 mm diameter and 3 mm thickness) was carried out using a SPS apparatus (515 model, Fuji Electronic Industrial Co. Ltd., Kanagawa, Japan) under vacuum conditions (20 Pa). This equipment combines a uniaxial press (max 50 kN) with a DC pulsed current generator (10 V, 1500 A, 300 Hz), to simultaneously apply an electric current across the processing powders and the graphite die containing them, together with a mechanical load through the die plungers. The temperature was measured using a k-type thermocouple inserted in a small hole drilled on the lateral die surface. The latter one was covered with a graphite felt to minimize heat losses by radiation.

During each SPS experiment, temperature was increased at a constant rate (100°C/min) from room to the maximum T_D level. Then, the dwell temperature was kept constant for 3 min, followed by the sample cooling step. In this work, the T_D value was varied in the range 600-900°C while the applied pressure (P) was 15 MPa

in all experiments. For the sake of reproducibility, each experiment was repeated at least twice.
After SPS, the obtained samples were ground, to remove residual graphite, using progressively finer abrasive paper down to 1000-grit. Densities of sintered specimens were measured by the Archimedes' method.
The samples' surface to be exposed to optical measurements was examined by high-resolution scanning electron microscopy (HR-SEM, mod. S4000, Hitachi, Tokyo, Japan) equipped with a UltraDry EDS detector (Thermo Fisher Scientific, Waltham, MA, USA). To estimate surface porosity of SPS samples, SEM micrographs were analyzed using the open source software GNU Image manipolation Program GIMP (version 2.8).
The spectral range 0.19-16.00 μm was considered for the optical property assessment, in order to characterize the sample interaction both with solar radiation (extraterrestrial spectrum) and with thermal radiation at various temperatures. To do that, hemispherical reflectance was measured using two instruments: a double-beam spectrophotometer (Perkin Elmer Lambda900) with a 150-mm diameter Spectralon®-coated integrating sphere for the spectral range 0.19-2.50 μm, and a Fourier Transform spectrophotometer (FT-IR Bio-Rad "Excalibur") with a gold-coated integrating sphere and a liquid N_2-cooled detector for the wavelength region from 2.5 to 16.0 μm. All the data have been taken for quasi-normal light incidence angle. For opaque materials, like in the case of these lunar regolith simulants, the spectral absorptance α(λ) is obtained from the spectral hemispherical reflectance ρ'∩(λ) according to the following relation:

$$\alpha(\lambda) = 1 - \rho' \cap (\lambda) \qquad (1)$$

and, according to the Kirchoff's law, it is equal to the spectral emittance ε(λ):

$$\alpha(\lambda) = \varepsilon(\lambda) \qquad (2)$$

Then, the total solar absorptance can be obtained as:

$$\alpha = \frac{\int_{\lambda min}^{\lambda MAX} \alpha(\lambda) \cdot I_{Sun}(\lambda) \cdot d\lambda}{\int_{\lambda min}^{\lambda MAX} I_{Sun}(\lambda) \cdot d\lambda} \qquad (3)$$

and the total thermal emittance at the temperature T as:

$$\varepsilon(T) = \frac{\int_{\lambda min}^{\lambda MAX} \varepsilon(\lambda) \cdot I_{BB,T}(\lambda) \cdot d\lambda}{\int_{\lambda min}^{\lambda MAX} I_{BB,T}(\lambda) \cdot d\lambda} \qquad (4)$$

where the integration boundaries λ_{min}= 0.19 μm, λ_{MAX}= 16 μm, correspond to the ones of the spectral range experimentally accessible in our case, $I_{Sun}(\lambda)$ is the extraterrestrial solar irradiance [30] and $I_{BB,T}(\lambda)$ is the blackbody irradiance at the temperature T.

3. Results and discussion

Lunar regolith powders were first characterized before being processed by SPS. XRD analysis indicates that the simulant basically consists of Aluminum Silicate Anorthite, Magnesium Iron Silicate Olivine and Calcium Magnesium Aluminum Titanium Silicate Clinopyroxene (**Figure 1**).

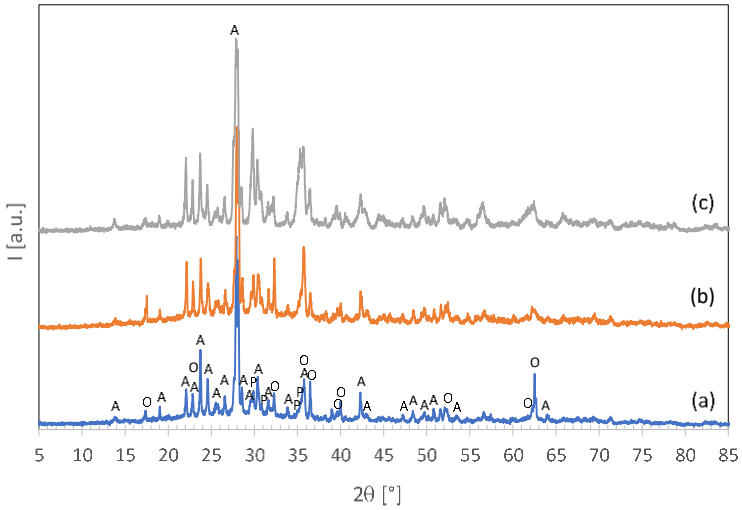

***Figure 1**. XRD patterns of (a) starting Lunar regolith simulant and corresponding SPS products obtained at (b) T_D= 700°C and (c) T_D= 900°C. A = Sodium Calcium Aluminum Silicate Anorthite, sodian disordered; O = Magnesium Iron Silicate Olivine; P = Calcium Magnesium Aluminum Titanium Silicate Clinopyroxene.*

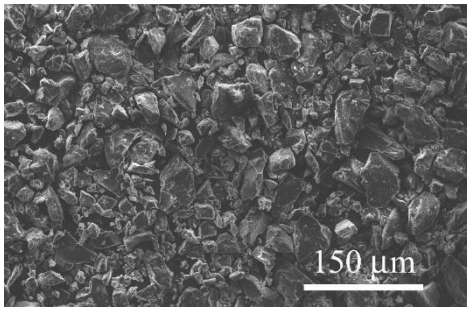

***Figure 2**. SEM micrograph of regolith powders to be consolidated by SPS.*

Figure 2 shows a SEM micrograph of the sieved powders, which evidenced that they consist of irregularly shaped particles with size less than 45 µm Moreover, laser scattering analysis provided the following particle size distribution parameters: d_{10}= 8.50±0.10 µm, d_{50}= 28.99±0.16 µm, d_{90} = 47.33±0.24 µm, and d_{av} =28.55±0.15 µm. The thermal stability of regolith from room temperature to 900°C was assessed by dynamic TGA tests, whose corresponding results are plotted in **Figure 3**. Only a negligeable weight change can be readily seen in such temperature interval.

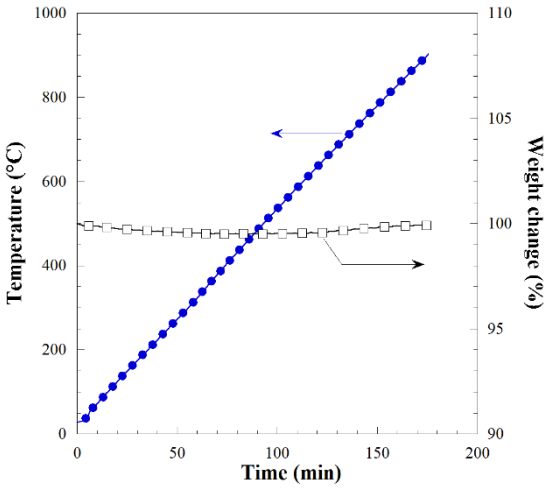

***Figure 3**. Weight change (%) of JSC-1A regolith during TGA experiment under dynamic conditions.*

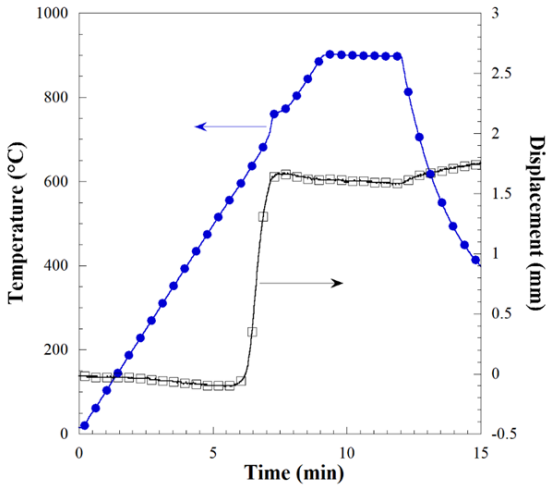

***Figure 4**. Sample displacement and corresponding temperature time profiles recorded during the consolidation by SPS of Lunar regolith powders for the case of T_D=900°C.*

Consolidation experiments were then conducted in the T_D range 600-900°C. Firstly, under the latter conditions, no evidence of melting phenomena occurrence is observed during SPS, which is consistent with the fact that the maximum temperature reached is well below the JSC-1A melting point (1100º - 1125º C). Other important information can be deduced when examining the example of SPS output reported in **Figure 4**. From this graph, no powder densification can be observed for temperature values below 600°C. In contrast, above the latter level, a significant change in sample displacement occurred up to 800°C. As the experiment proceeded, a slight reduction

of this parameter is recorded during the remaining non-isothermal step as well as when the sample is maintained for 3 min at 900°C. As discussed later, when samples density data will be considered, the latter outcome does not mean that regolith consolidation is complete at 800°C. Such decrease can be explained by the fact that the thermal expansion contribution to the recorded displacement overcomes, in the 800-900°C interval, that one due to sample densification.

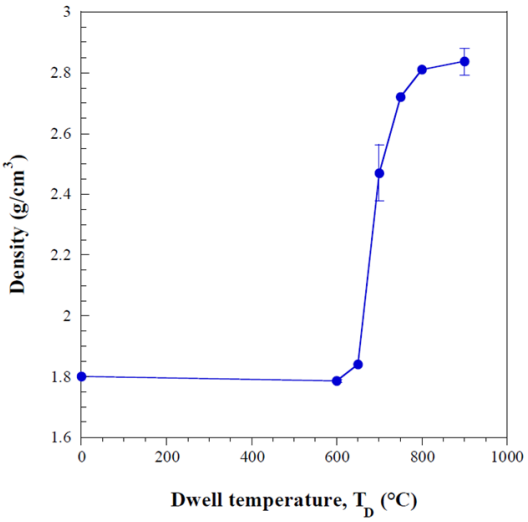

***Figure 5**. Effect of sintering temperature on the density of bulk Lunar regolith samples produced by SPS.*

The effect of the dwell temperature on the densification of JSC-1A regolith powders can be deduced from **Figure 5**. Consistently with displacement data examined previously (**Figure 4**), it is confirmed that no improvement in sample density occurs up to 600°C, whereas it markedly increases as the T_D value is progressively raised to 800°C. As the temperature was further augmented to 900°C, only a slight density increase was observed. The density value measured under the latter conditions was 2.84 ± 0.04 g/cm^3, corresponding to about 98 %.

To check if possible compositional changes in the regolith material took place during SPS, the XRD patterns of the sintered samples produced at 700 (relative density of about 86%) and 900°C are compared in **Figure 1** with that one relative to the original powders. No additional phases are detected by this analysis after SPS, except for the relative intensity of XRD peaks. In particular, Olivine peaks become less intense in XRD patterns of SPS samples, whereas a relative increase of Anorthite signals intensity is correspondingly observed.

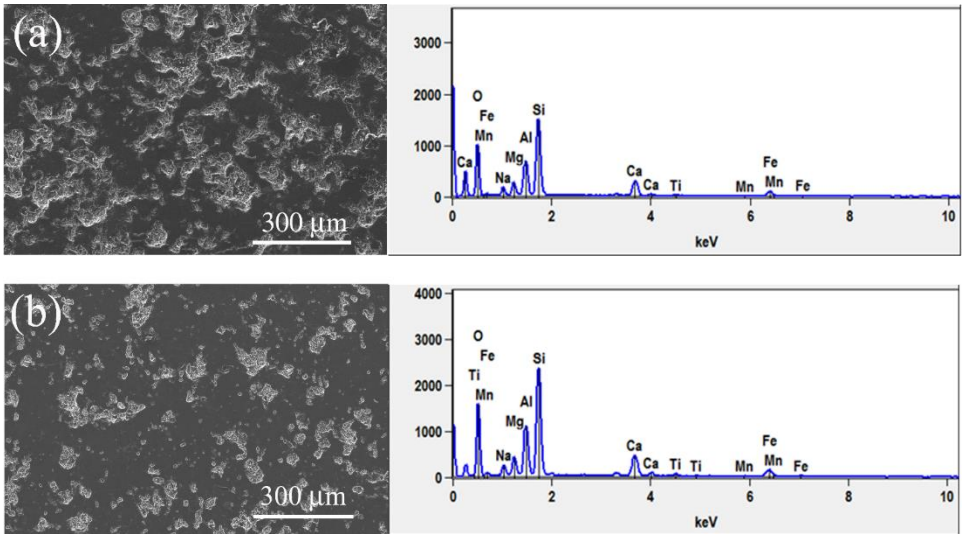

Figure 6*. SEM micrograph and corresponding EDX analysis spectra of SPS samples obtained at (a) 700 and (b) 900° C from regolith powders.*

Two SEM micrographs of the surface of bulk samples obtained by SPS at 700 and 900°C are shown in **Figure 6(a)** and **6(b)**, respectively. A significant difference in surface porosity of the two samples is evidenced by these images, which rather agrees with density data plotted in **Figure 5**. In this regard, the surface porosity values, estimated by image analysis, of bulk spark plasma sintered specimens produced at 700 and 900°C are 10.27±1.24, and 5.87±1.65 vol.%, respectively. It should be noted that the latter values likely exceed the porosity levels in the corresponding bulk materials, since some larger surface pores are probably due to grain pulling-out phenomenon occurring during the polishing procedure. Image analysis carried out on the sample processed at 900°C revealed that approximately 50 % porosity is due to pores less than 5 µm sized, whereas about 12 % of this characteristic can be ascribed to pores larger than 30 µm. On the other hand, about 50 % porosity present on the surface of the regolith specimen sintered at 700°C corresponds to 10-20 µm sized pores, while 12% and 8% of this characteristic are ascribed to those with 30 µm and 40-45 µm, respectively.

The most significant elements present in the sintered materials are evidenced by EDS analysis, whose corresponding spectra are also reported in **Figure 6**. As expected, Si, Al, Mg, Ca and O are the predominant elements detected by this analysis, along with some minor species (Fe, Ti, Mn, Na etc.).

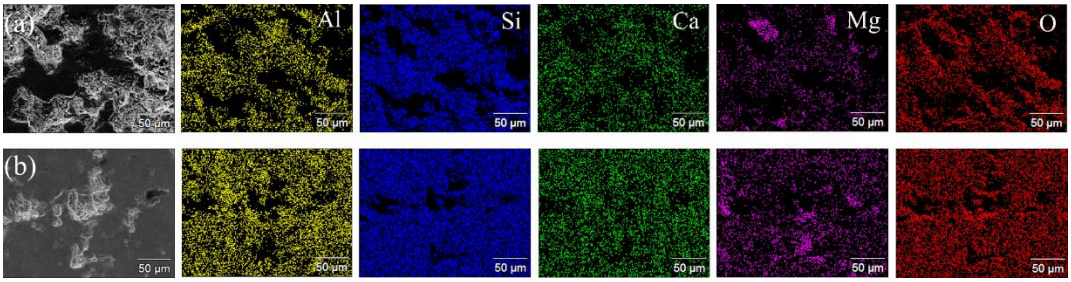

Figure 7*. EDX compositional maps and corresponding SEM micrographs of SPS samples obtained at (a) 700 and (b) 900° C from Lunar regolith powders.*

More detailed information on product composition and homogeneity are provided by **Figure 7**, where the Si, Al, Mg, Ca and O EDX maps are shown. All these elements are distributed quite uniformly across the material, with the only exception for some Mg-rich silicate regions ascribed to Magnesium Iron Silicate Olivine.
Absorptance spectra, calculated from Eqs. 1-2, are shown in **Figure 8**. Both sintered samples are characterized by a generally higher value of spectral absorptance with respect to the powder sample, with values in the range 0.82-0.99. As expected from the presence of the same minerals in both samples, both curves show similar positions of absorptance maxima/minima. Their different relative peak heights could be ascribed to diverse amounts of the individual minerals, combined with spectral distortions due to the dissimilar samples' porosities. In fact, the observed pore size distributions might qualitatively justify the most apparent spectral differences in terms of radiation trapping within the surface pores [31]. In particular, the sample sintered at 900°C, which has generally smaller pores with half of them smaller than 5 µm, shows a higher absorptance for wavelengths shorter than about 5-6 µm, while the other sample, whose pores mainly have a 10-20 µm size, show a higher absorptance in the corresponding wavelength range. The spectral absorptance of the powder is lower and ranges from about 0.6 to 0.9. The peak around 8 um, shown by all samples, could be ascribed to silicates [32].

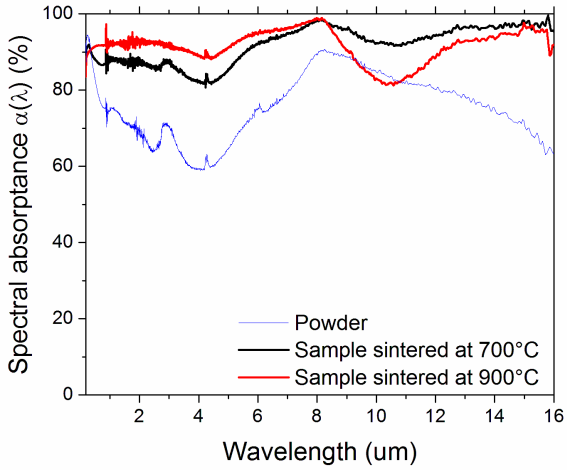

Figure 8: *Absorptance spectra of sintered specimens and the reference powder sample.*

Figure 9 shows the values of temperature-dependent integrated emittance. The minimum temperature has been chosen 100K, representative of the night temperature value on the lunar equatorial surface [33]. In addition, we explicitly took into account the temperature value of 250K, which is near to the almost constant temperature of lunar regolith about 0.3-0.5 m below the surface [2], Another key temperature value is around 400K, corresponding to the maximum temperature at the equatorial belt [33]. For the technological applications of interest in the present work, namely solar energy harvesting and sensible-heat thermal energy storage [3], the materials should be subjected to significantly higher temperatures. Therefore, in our analysis, we extended the considered temperature range up to 1300K, which is slightly lower than the melting temperature of the regolith simulant declared by the supplier.

When in powdered form, the regolith simulant appears to have consistently lower solar absorptance and thermal emittance at all temperatures, in comparison to sintered specimens. Its maximum value of thermal emittance, 0.80, is expected at 300K, while this parameter decreases to 0.73 at 100K and 0.69 at 1100K. Sintered pellets show absorptance values of 0.88 and 0.92 (samples sintered at 700°C and 900°C, respectively), with emittance values in the range 0.96-0.87 (T_D=700°C) and 0.93-0.91 (T_D= 900°C). In addition, they exhibit different temperature-dependent trends. Indeed, when considering the sample sintered at 700°C, emittance decreases at increasing temperatures, whereas only minor changes are correspondingly observed for the pellet sintered at 900°C. The knowledge of these trends allows to identify the materials' potential for intended applications, as well as optimal operating conditions to be adopted.

The ISRU paradigm is of paramount importance in any scenario of planetary exploration and future manned or robotic colonization. Sunlight is the available energy source, which needs to be collected, stored, and used both in form of heat and electricity. Regolith, either native or once processed to produce sintered bricks and bulks, is the natural candidate material to be used and adapted to most energy needs. In a possible energy generation scheme, solar collectors on the Moon or planetary object surface harvest sunlight and concentrate it into solar absorbers constituted by sintered regolith blocks exchanging heat with some heat transfer medium. On the

Moon, sensible-heat thermal energy storage units could be made by processed regolith as well [3], and buried under the surface to benefit of the thermally insulating characteristics of the surrounding powdered regolith. The use of the same starting material to be tailored, by means of optimized processing approaches, for various applications, is a formidable challenge to which the present work aims to bring its contribution.

For both solar absorber and thermal energy storage applications, a key point is represented by the high thermal conductivity. To this regard, it has been demonstrated a 200-fold increase of thermal conductivity of a sintered regolith simulant with respect to the native material [3]. Obviously, optical properties are also of extreme importance, in what concerns the interaction with both solar and thermal radiation.

As for solar absorber application, the ideal material should possess, at the operating temperature, a high solar absorptance and the lowest thermal emittance as possible. With a properly dimensioned sunlight collecting system, the working temperature of the absorber is quickly reached and steadily maintained during the illumination period, e.g., the lunar day only. In this sense, the system is similar to solar receivers on Earth, with the advantage of the absence of thermal losses due to conductive and convective heat exchanges with the surrounding atmosphere. First of all, it should be noticed that sintered pellets show a higher solar absorptance than native powders (see legends in **Figure 9**). Therefore, they result more suitable to be employed for solar receivers in architectures with a cavity-like solar receiver. For operating temperatures lower than 1000K, the sample sintered at 900°C appears the most promising, due to the highest solar absorptance and lowest thermal emittance. At 1000K both pellets show the same spectral selectivity value, while, beyond such temperature level, the sample sintered at 700°C shows lower emittance. As the latter specimen is also characterized by a lower solar absorptance, system-specific evaluations should be made case by case, according to the system architecture, to identify the most suitable material depending on the working temperature. As for the untreated powdered regolith, it could be considered to be used in solar receivers only within significantly more complex architectures using fluidized-bed approaches, where the powder could constitute at the same time the solar absorbing, heat transfer and heat storage medium. However, the solar absorption efficiency in this case would be poorer, because the absorptance of powder regolith is consistently lower than that of sintered pellets. Moreover, a number of technical difficulties have to be overcome to implement a fluidized-bed architecture in an extra-terrestrial environment (e.g., the need of a transparent window for the powder container - hard to fabricate with ISRU - the energy consumption to maintain the powder in fluidized conditions, etc.). On the other hand, the high reflectance displayed by powdered regolith-covering the Moon could be suitably exploited to allow the highly-absorbing sintered receiver material to harvest and recover some of sunlight radiation reflected by its surface**.**

For buried sensible-heat TES applications, the material should operate between its maximum allowable temperature (melting temperature in the range 1100-1125°C) and 250 K, with thermal cycles corresponding to the day-night cycles. The most relevant optical parameter here is the thermal emittance only. Showing the lowest emittance for temperatures higher than 500K (**Figure 9**), the ceramic sintered at 700°C results therefore the best option with respect to the other processed pellet. Powdered regolith emittance would actually show an even lower emittance, but its

poor thermal conductivity would make difficult the actual usage as heat storage medium.

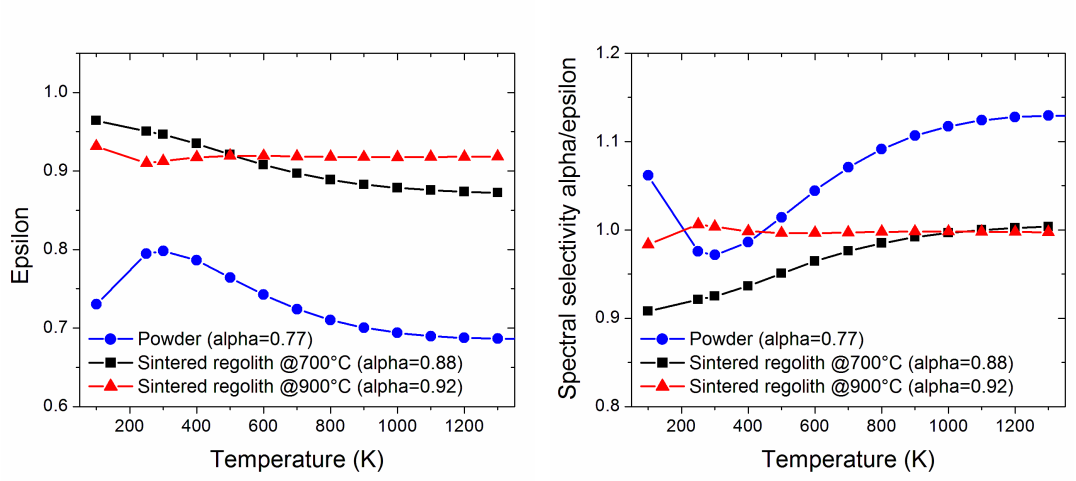

Figure 9: *Integrated thermal emittance (left) and spectral selectivity (right) of investigated materials as a function of the temperature.*

4. Conclusions

In this work, taking a lunar regolith simulant as a case-study, we assessed the potential of sintered regolith for solar energy harvesting and thermal energy storage within an ISRU perspective, by evaluating how optical properties of both sintered and pristine regolith powders could be used for solar radiation absorption, thermal radiation management and thermal energy storage.

To this aim, simulant regolith powders have been first sintered for 3 min at 700-900°C (100°C/min heating rate), in vacuum (20 Pa), under a mechanical pressure of 15 MPa. The obtained pellets, which show relative densities of approximately 86 and 98%, respectively, have been then characterized from compositional and microstructural points of view. No additional phases have been detected after SPS compared to original powder. Optical properties (spectral absorptance/emittance, integrated solar absorptance and integrated thermal emittance estimated from 100 to 1300K temperature) have been evaluated for samples sintered at 700°C and 900°C, and thoroughly discussed. Similarly to what already reported in the literature for thermophysical properties, we proved that powder sintering changed the optical properties of regolith in a process-dependent way. Specifically, the process parameter investigated in the present study, the sintering temperature, is generally found to increase spectral absorptance/emittance with respect to pristine powders. Integrated solar absorptance and thermal emittance at all considered temperatures resulted therefore enhanced.

These results open interesting perspectives for ISRU applications, allowing to exploit the different properties of both pristine powders and their sintered bricks, as well as of the proper interplay among them. In a more general ISRU framework, the approach described in this work can be extended to other planetological environments where regolith can be found (other natural satellites, asteroids, planets), once the specific differences with the Moon in terms of regolith characteristics (composition, granulometry, maturity, etc) and astronomical

properties (size, rotational period, distance from the Sun, etc) are taken into account.

Acknowledgments
Mr. M. D'Uva and Mr. M. Pucci (both from CNR-INO) are gratefully acknowledged for technical assistance in the optical measurements experimental setup. G.C. acknowledges the results obtained in this manuscript as quite important for the "Generazione E" project, sponsored by the Italian Ministry of Education, University and Research, Italy (Cod. CUP: B96G18000560005).

References

[1] M. Kaczmarzyk, M. Gawronski, and G. Piatkowski, “Global database of direct solar radiation at the Moon’s surface for lunar engineering purposes.,” in *E3S Web of Conferences (Vol. 49, p. 00053)*, 2018.

[2] M. F. Palos, P. Serra, S. Fereres, K. Stephenson, and R. González-Cinca, “Lunar ISRU energy storage and electricity generation.,” *Acta Astronaut.*, vol. 170, pp. 412–420, 2020.

[3] P. Fleith *et al.*, “In-situ approach for thermal energy storage and thermoelectricity generation on the Moon: Modelling and simulation.,” *Planet. Sp. Sci.*, vol. 181, p. 104789, 2020.

[4] Gaffey M.J. and T. B. McCord, “Mineralogical and petrological characterizations of asteroid surface materials,” in *Asteroids. (A80-24551 08-91) Tucson, Ariz.*, University of Arizona Press, 1979, pp. 688–723.

[5] J. S. Kargel, “Metalliferous asteroids as potential sources of precious metals,” *J. Geophys. Res.*, vol. 99, E10, pp. 21129–21142, 1994.

[6] J. C. Sercel *et al.*, “Practical Applications of Asteroidal ISRU in Support of Human Exploration,” in *Primitive Meteorites and Asteroids*, N. Abreu, Ed. Elsevier, 2018, pp. 477–524.

[7] S. J. Ostro *et al.*, “Asteroid 1986 DA: Radar Evidence for a Metallic Composition,” *Science (80-.).*, vol. 252, pp. 1399–1404, 1991.

[8] J. A. Sanchez *et al.*, “Physical Characterization of Metal-rich Near-Earth Asteroids 6178 (1986 DA) and 2016 ED85,” *Planet. Sci. J.*, vol. 2, p. 205, 2021.

[9] A. Dell’Oro and P. Paolicchi, “Statistical properties of encounters among asteroids: a new, general purpose, formalism,” *Icarus*, vol. 136, pp. 328–339, 1998.

[10] A. Dell’Oro, “Statistics of impacts among orbiting bodies: a Monte Carlo approach,” *Mon. Not. R. Astron. Soc.*, vol. 467, pp. 4817–4840, 2017.

[11] M. Delbo, A. Dell’Oro, A. W. Harris, S. Mottola, and M. Mueller, “Thermal inertia of near-Earth asteroids and implications for the magnitude of the Yarkovsky effect,” *Icarus*, vol. 190, pp. 236–249, 2007.

[12] M. S. Hammond, J. E. Good, S. D. Gilley, and R. W. Howard, “Developing fabrication technologies to provide on demand manufacturing for exploration of the Moon and Mars,” in *Collection of Technical Papers, 44th AIAA Aerospace Sciences Meeting 9*, 2006, pp. 6353–6360.

[13] J. T. Howell, J. C. Fikes, C. A. McLemore, and J. E. Good, “On-site fabrication infrastructure to enable efficient exploration and utilization of space,” in *International Astronautical Federation - 59th International Astronautical Congress 2008 12*, 2008, pp. 7842-7848.

[14] X. Zhang *et al.*, “Microstructure evolution during spark plasma sintering of FJS-1 lunar soil simulant,” *J. Am. Ceram. Soc.*, vol. 103, pp. 899–911, 2020.

[15] A. Zocca, M. Fateri, D. Al-Sabbagh, and J. Günster, “Investigation of the sintering and melting of JSC-2A lunar regolith simulant,” *Ceram. Int.*, vol. 46, pp. 14097–14104, 2020.

[16] C. Allen, J. Graf, and D. McKay, “Sintering Bricks on The Moon,” in *Engineering, Construction, and Operations in Space IV (pp.). ASCE.*, American Society of Civil Engineers, 1994, pp. 1220–1229.

[17] L. A. Taylor and T. T. Meek, “Microwave sintering of lunar soil: Properties, theory, and practice,” *J. Aerosp. Eng.*, vol. 18, pp. 188–196, 2005.
[18] Y.-J. Kim, B.-H. Ryu, H. Woo Jin, J. Lee, and H.-S. Shin, “Microwave Sintering of Lunar Regolith Simulant for Manufacturing Building Elements,” in *Earth and Space 2021: Space Exploration, Utilization, Engineering, and Construction in Extreme Environments - Selected Papers from the 17th Biennial International Conference on Engineering, Science, Construction, and Operations in Challenging Environments*, 2021, pp. 985–991.
[19] C. White, F. Alvarez, and Shafirovich, “Combustible mixtures of lunar regolith with metals: Thermodynamic analysis and combustion experiments,” *J. Thermophys. Heat Transf.*, vol. 25, pp. 620–625, 2011.
[20] G. Corrias, R. Licheri, R. Orrù, and G. Cao, “Self-propagating high-temperature reactions for the fabrication of Lunar and Martian physical assets,” *Acta Astronaut.*, vol. 70, pp. 69–76, 2012.
[21] G. Corrias, R. Licheri, R. Orrù, and G. Cao, “Optimization of the self-propagating high-temperature process for the fabrication in situ of Lunar construction materials,” *Chem. Eng. J.*, vol. 193, pp. 410–421, 2012.
[22] C. Alvarez, F., A. K. White, N. Swamy, and E. Shafirovich, “Combustion wave propagation in mixtures of JSC-1A lunar regolith simulant with magnesium,” in *Proceedings of the Combustion Institute vol. 34*, 2013, pp. 2245–2252.
[23] K. Oh, H. Yi, T. Chen, B. J. Chow, R. Kou, and Y. Qiao, “Impact formation of ultralow-binder-content composite ‘lunar cement,’” *CEAS Sp. J.*, vol. 13, pp. 183–187, 2021.
[24] T. Chen, B. J. Chow, and M. Wang, “High-pressure densification of composite lunar cement,” *J. Mater. Civ. Eng.*, vol. 29, p. 06017013, 2017.
[25] X. L. Phuah, H. Wang, B. Zhang, J. Cho, X. Zhang, and H. Wang, “Ceramic material processing towards future space habitat: Electric current-assisted sintering of lunar regolith simulant,” *Materials (Basel).*, vol. 13, p. 4128, 2020.
[26] X. Zhang *et al.*, “Spark plasma sintering of a lunar regolith simulant: effects of parameters on microstructure evolution, phase transformation, and mechanical properties,” *Ceram. Int.*, vol. 47, pp. 5209–5220, 2021.
[27] M. Fateri *et al.*, “Solar Sintering for Lunar Additive Manufacturing,” *J. Aerosp. Eng.*, vol. 32, p. 04019101, 2019.
[28] A. Meurisse, A. Makaya, C. Willsch, and M. Sperl, “Solar 3D printing of lunar regolith,” *Acta Astronaut.*, vol. 152, pp. 800–810, 2018.
[29] G. Cao, C. Estournés, J. Garay, and R. Orrù, Eds., *Spark Plasma Sintering: Current Status, New Developments and Challenges.* Elsevier, 2019.
[30] “ASTM E490-00a, Standard Solar Constant and Zero Air Mass Solar Spectral Irradiance Tables,.” ASTM International, West Conshohocken, PA, 2019.
[31] E. Sani, D. Sciti, L. Silvestroni, A. Bellucci, S. Orlando, and D. M. Trucchi, “Tailoring optical properties of surfaces in wide spectral ranges by multi-scale femtosecond-laser texturing: A case-study for TaB2 ceramics,” *Opt. Mater. (Amst).*, vol. 109, p. 110347, 2020.
[32] J. E. Conel, “Infrared emissivities of silicates: Experimental results and a cloudy atmosphere model of spectral emission from condensed particulate mediums,” *J. Geophys. Res.*, vol. 74, pp. 1614–1634, 1969.

[33] R. B. Malla and K. M. Brown, “Determination of temperature variation on lunar surface and subsurface for habitat analysis and design,” *Acta Astronaut.*, vol. 107, pp. 196–207, 2015.